

## Chemical-Potential Measurements and Phase Diagram of a Pseudoternary Solid: $\text{Li}_x\text{Cu}_y\text{Mo}_6\text{S}_8$

C. C. H. Jui,<sup>(a)</sup> W. R. McKinnon, and J. R. Dahn

*Solid State Chemistry, Chemistry Division, National Research Council of Canada, Ottawa K1A 0R9, Canada*  
(Received 22 October 1984)

By use of x-ray-diffraction and electrochemical techniques we have measured the phase diagram of the pseudoternary solid,  $\text{Li}_x\text{Cu}_y\text{Mo}_6\text{S}_8$ . We compare our measurements of the Li chemical potential,  $\mu$ , and the response function  $-(\partial x/\partial \mu)_{y,T}$  near phase boundaries to predictions of theory.

PACS numbers: 64.60.Cn, 61.60.+m, 64.70.Kb

Intercalation compounds with one type of guest atom are pseudobinary systems as long as the host retains its structure, and the behavior of such compounds can often be understood with two-component models.<sup>1,2</sup> One component is then the guest and the other is the interstitial site where the guest resides. Similarly, intercalation compounds with two types of guests are pseudoternary systems. Adding the second guest should complicate and enrich the behavior of intercalation systems just as adding a third component to a binary alloy<sup>3</sup> or to a binary fluid<sup>4</sup> does. The presence of two mobile guests can lead to surprises, because even if the average concentration of one of the guests is fixed, that guest can segregate in the host so that its local concentration varies. A complete understanding of these systems requires a pseudoternary phase diagram, a phase diagram presented as a function of the concentration of both guests. Here we present such a phase diagram for  $\text{Li}_x\text{Cu}_y\text{Mo}_6\text{S}_8$  [Fig. 1(a)], the first for any intercalation compound.

Although phase diagrams of ternary and pseudoternary systems ( $A_xB_yC_{1-x-y}$ ) have been measured<sup>5</sup> and calculated,<sup>6,7</sup> the chemical potentials  $\mu$  and  $\nu$  of the components  $A$  and  $B$  have not been measured. In addition, there is no theoretical treatment of the behavior of response functions like  $(\partial x/\partial \mu)_{y,T}$  near critical points of ternary systems. We have used electrochemical techniques<sup>8</sup> to measure the chemical potential,  $\mu$ , of Li in  $\text{Li}_x\text{Cu}_y\text{Mo}_6\text{S}_8$ , as well as  $(\partial x/\partial \mu)_{y,T}$ . We show how knowing  $\mu$  simplifies the measurement of the phase diagram. We also present the first measurement of the chemical potentials of all the coexisting phases in any ternary or pseudoternary solid. These are shown in Fig. 1(b) for  $\text{Li}_x\text{Cu}_y\text{Mo}_6\text{S}_8$ .

The phase diagram [Fig. 1(a)] was determined by isothermal cuts at constant  $y$ . We intercalate Li into  $\text{Cu}_y\text{Mo}_6\text{S}_8$  using  $\text{Li}/\text{Li}_x\text{Cu}_y\text{Mo}_6\text{S}_8$  electrochemical cells while monitoring the cell's voltage,  $V(x)$ .<sup>8</sup> We correlate  $-(\partial x/\partial \mu)_{y,T}$ , calculated from  $V(x)$ , with the structure of  $\text{Li}_x\text{Cu}_y\text{Mo}_6\text{S}_8$  measured *in situ* by use of cells with x-ray windows.<sup>9</sup> For samples with two phases, we determined the fraction of the sample in phase 1 ( $f$ ) and 2 ( $1-f$ ) from the intensities of the Bragg peaks. Thus for a single cut across the phase di-

agram we can measure  $x$ ,  $f$ , and  $V(x)$  at a fixed  $y$ . Figure 2 shows an example of our results for  $y=2$ . Here, as Li intercalates, the sample changes from a single phase to a two-phase mixture and back again to

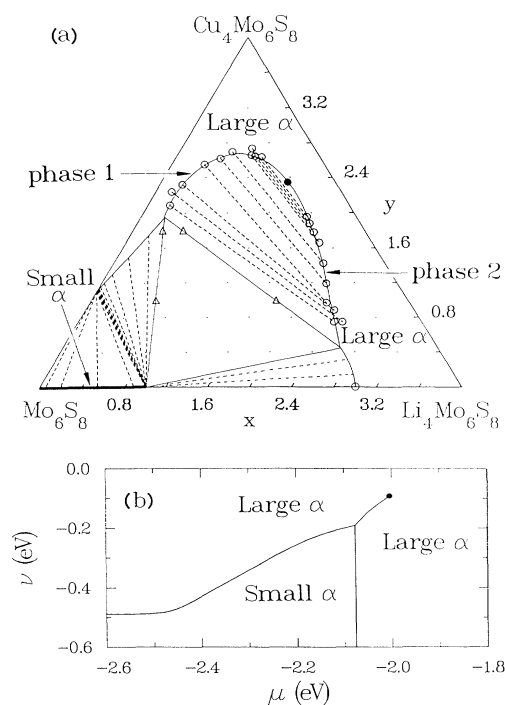


FIG. 1. Room-temperature phase diagram of  $\text{Li}_x\text{Cu}_y\text{Mo}_6\text{S}_8$  plotted (a) vs composition and (b) vs chemical potentials of lithium ( $\mu$ ) and copper ( $\nu$ ) relative to the pure elements. The solid dot is a critical point, solid lines are phase boundaries, and the dashed lines in (a) are tie lines. The open circles are tie-line endpoints determined from x-ray and electrochemical results and the triangles are the boundaries of the three-phase region measured electrochemically. The rest of the phase diagram was inferred from x-ray and electrochemical data. Single-phase regions with large and small rhombohedral angle  $\alpha$  have been indicated. Phases 1 and 2 (referred to in Fig. 2) lie on the phase boundary but are separated by the critical point. The triclinic and incommensurate phases of  $\text{Li}_x\text{Mo}_6\text{S}_8$  near  $x=4$  (Ref. 12) have been omitted for clarity.

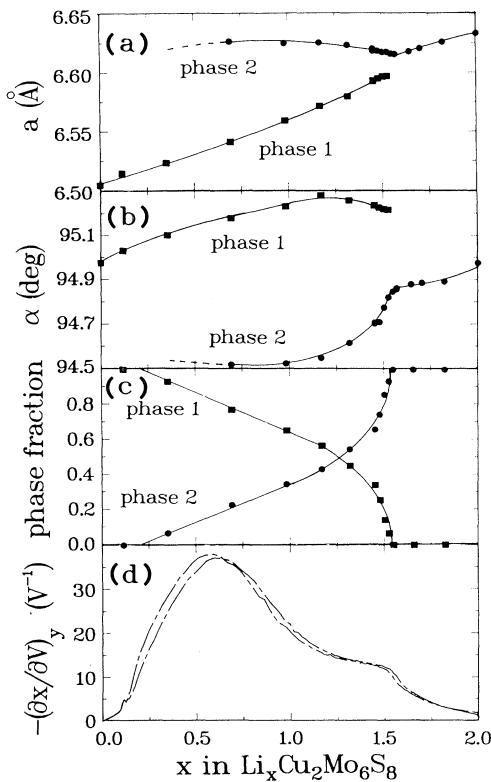


FIG. 2. Lattice parameters, phase fractions, and  $-(\partial x/\partial V)_{y,T}$  for  $\text{Li}_x\text{Cu}_2\text{Mo}_6\text{S}_8$ .

a single phase. Figures 2(a) and 2(b) show the lattice parameters, Fig. 2(c) shows the fractions of the two phases present, and Fig. 2(d) shows  $-(\partial x/\partial V)_{y,T}$ .

Coexisting phases have the same  $\mu$  and copper chemical potential  $\nu$ .<sup>3</sup> Thus all points  $(x,y)$  on the line (called the tie line) joining two coexisting phases  $(x_1,y_1)$  and  $(x_2,y_2)$  have the same  $\mu$  and  $\nu$  and, hence, the same  $V$ . By measuring  $x$  and  $f$  for 2 samples with different  $y$  but at the same  $V$ , we can calculate the endpoints  $x_1, y_1$ , and  $x_2, y_2$  for a single tie line. Further details will be published later.

As in pseudobinary intercalation compounds,<sup>1</sup> structure in  $-(\partial x/\partial V)_{y,T}$  can indicate phase transitions. Figure 3 shows  $-(\partial x/\partial V)_{y,T}$  versus  $V$  for  $y=1, 2$ , and 3. For  $y=3$ , no anomalies are seen;  $\text{Li}_x\text{Cu}_y\text{Mo}_6\text{S}_8$  is a single phase for  $0 < x < 1$ .<sup>10</sup> The steps in  $-(\partial x/\partial V)_{y,T}$  at 2.002 and 2.060 V for  $y=2$  result because the sample is two-phase between these voltages and single-phase elsewhere. For  $y=1$  the large peak near 2.08 V indicates a three-phase region ( $\mu$  and  $\nu$  are constant when three phases coexist<sup>3</sup>). The endpoints of the corresponding plateau in  $V(x)$  determine the limits of the three-phase region. Thus the phase boundaries can be obtained from electrochemical data alone in some cases.

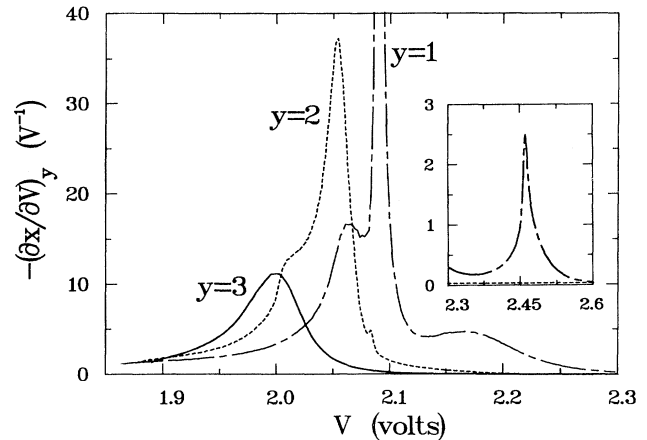


FIG. 3.  $-(\partial x/\partial V)_{y,T}$  for  $\text{Li}/\text{Li}_x\text{Cu}_y\text{Mo}_6\text{S}_8$  cells with  $y=1, 2, 3$ .

Using data for  $y=1, 1.8, 2, 2.3, 2.5$ , and 3, and previous work on  $\text{Cu}_y\text{Mo}_6\text{S}_8$ <sup>11</sup> and  $\text{Li}_x\text{Mo}_6\text{S}_8$ ,<sup>12</sup> we constructed Fig. 1(a). Figure 1(b) was calculated by use of the tie lines in Fig. 1(a),  $V$  for these tie lines, and

$$dv/d\mu = -(x_2 - x_1)/(y_2 - y_1), \quad (1)$$

which is a Clausius-Clapyron relation.<sup>13</sup>  $dv/d\mu$  is the local slope of the coexistence curve. In Fig. 1(b),  $\mu$  and  $\nu$  are measured with respect to Li and Cu metal, respectively. Figure 1 shows a critical or binodal point and a triple point or three-phase region.

The coexistence curves in Fig. 1 separate the  $\mu$ - $\nu$  plane into regions of small and large values of the rhombohedral angle,  $\alpha$ . In  $\text{Li}_x\text{Mo}_6\text{S}_8$   $\alpha$  varies between 91.25 and 92.30° for  $0 < x < 1$ ,<sup>12</sup> whereas all other single-phase compositions of  $\text{Li}_x\text{Cu}_y\text{Mo}_6\text{S}_8$  have  $\alpha > 93.7$ .<sup>10-12,14</sup> Most Chevrel compounds fall into two such classes with large (93-96) and small (88-92)  $\alpha$ .<sup>15</sup> For small  $\alpha$ , compounds  $A_x\text{Mo}_6\text{S}_8$  have  $x < 1$  and the  $A$  atoms occupy sites centered on the  $\bar{3}$  axis at the origin of the unit cell.<sup>15</sup> For  $\alpha > 93$ , the single site splits into a hexagon of sites and the guest atoms also occupy other sites, and so  $x$  can be greater than 1. We believe that the two regions in Fig. 1(b) correspond to these two geometries. There are first-order transitions (two-phase regions) which must be crossed to go from small to large  $\alpha$ . [These may be similar to the transition from small to large  $\alpha$  in  $\text{InMo}_6\text{S}_x\text{Se}_{8-x}$ .<sup>16</sup>] The transitions extend from  $x=1$  to  $x=3$  in  $\text{Li}_x\text{Mo}_6\text{S}_8$  and from  $y=0$  to  $y=1.1$  in  $\text{Cu}_y\text{Mo}_6\text{S}_8$  and propagate inward to form two sides of the three-phase region in Fig. 1(a). The third side is bounded by a two-phase region (here both phases have  $\alpha > 94$ ) which terminates in a critical point.

As an example of how the miscibility gap on this third side might form, consider a regular-solution model<sup>6</sup> for  $\text{Li}_x\text{Cu}_y\text{Mo}_6\text{S}_8$ . We write the free energy,  $F$ ,

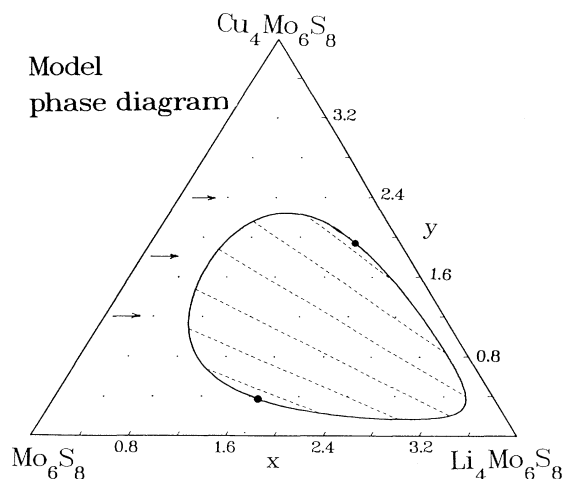


FIG. 4. Phase diagram calculated as described in the text. The solid dots are critical points.

as

$$F/NkT = auv + buz + cvz + u \ln(u) + v \ln(v) + z \ln(z) \quad (2)$$

where  $u = x/4$ ,  $v = y/4$ ,  $z = l - u - v$ ,  $k$  is Boltzmann's constant, and  $N$  is the number of lattice sites.  $a$ ,  $b$ , and  $c$  are interactions between Li and Cu, Li and empty sites, and Cu and empty sites, respectively. Figure 4 shows a phase diagram calculated by methods described in Ref. 7 for  $a = b = 0$  and  $c = -10$ . This is not meant to reproduce Fig. 1(a), but to show how a miscibility gap can be caused by pairwise interactions. These particular interactions give a miscibility gap that does not touch any of the sides of the triangle and has tie lines with directions similar to those for large  $x$  and  $y$  in Fig. 1(a). The direction of the tie lines plays a role in determining  $-(\partial x/\partial V)_{y,T}$  in the two-phase region. Only when the tie lines in the experiment and in the model have similar direction does  $-(\partial x/\partial V)_{y,T}$ , calculated in the two-phase region, show the same general features as experiment.

We calculated  $-(\partial x/\partial V)_{y,T}$  for  $y = 2.4$ , 1.8, and 1.2 (shown in Fig. 5) for this model. Note the steps in  $-(\partial x/\partial V)_{y,T}$  for  $y = 1.8$  and 1.2 when the two-phase boundary is crossed, similar to the data for  $y = 2$  in Fig. 3. The steps are not an artifact of mean-field theory. For points infinitesimally separated by the phase boundary,

$$\begin{aligned} (\partial x/\partial \mu)_y(2\text{-phase}) - (\partial x/\partial \mu)_y(1\text{-phase}) \\ = (\partial y/\partial v)_\mu [dv/d\mu - (\partial v/\partial \mu)_y]^2. \end{aligned} \quad (3)$$

$dv/d\mu$  is again the local slope of the coexistence curve. Since  $(\partial y/\partial v)_\mu$  is always positive  $(\partial x/\partial \mu)_y$  always steps up when the two-phase region is entered.

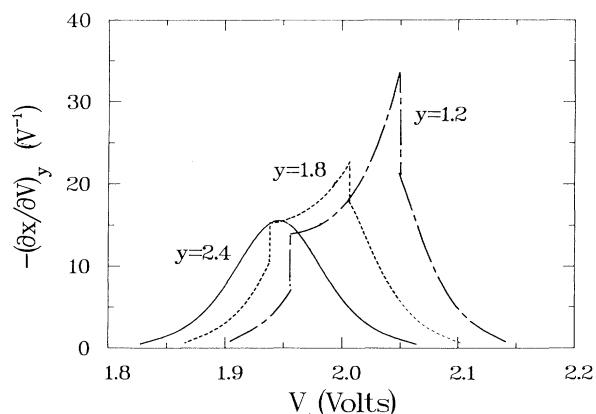


FIG. 5.  $-(\partial x/\partial V)_{y,T}$  calculated for cuts across the phase diagram in Fig. 4 at  $y = 2.4$ , 1.8, and 1.2 (arrows in Fig. 4).

Mean-field theory predicts a step in  $-(\partial x/\partial V)_{y,T}$  even at the critical point, but general arguments of Griffiths and Wheeler<sup>17</sup> predict that  $-(\partial x/\partial V)_y$  could diverge there. Experiments with  $y = 2.3$  near the critical point showed no evidence for such divergences. The transition might be a mean-field one because of the long-range strain fields caused by the appreciable lattice parameter mismatch of the coexisting phases [Figs. 2(a) and 2(b)]. Alternatively, the absence of a divergence could be related to the rounding of the data in Fig. 3 near the transition. This rounding might be due to the finite size of the powder grains studied (2–20 microns). It might also be due to differences between  $y$  or  $v$  between powder grains because there is no way for copper to migrate between grains. However, sintering pressed pellets of  $\text{Cu}_{2.5}\text{Mo}_6\text{S}_8$  powder at 1250°C did not improve the sharpness of the transitions.

(a) Present address: Department of Physics, University of Ottawa, Ottawa, Canada.

<sup>1</sup>W. R. McKinnon and R. R. Haering, *Mod. Aspects Electrochem.* **15**, 235 (1983).

<sup>2</sup>S. T. Coleman, W. R. McKinnon, and J. R. Dahn, *Phys. Rev. B* **29**, 4147 (1984).

<sup>3</sup>P. Haasen, *Physical Metallurgy* (Cambridge Univ. Press, Cambridge, England, 1978).

<sup>4</sup>A. W. Francis, *Liquid-Liquid Equilibria* (Wiley, New York, 1963).

<sup>5</sup>E. Raub and A. Engel, *Z. Metallkd.* **38**, 11 (1947); F. A. H. Schreinemakers and H. W. Bakhuis-Roozeboom, *Die heterogenen Gleichgewichte* (Viewig, Brunswick, 1911), Vol. 3, Pt. 2.

<sup>6</sup>J. L. Meijering, *Philips Res. Rep.* **5**, 333 (1950).

<sup>7</sup>R. Kikuchi, *Acta Metall.* **25**, 195 (1977).

<sup>8</sup>J. R. Dahn and W. R. McKinnon, *J. Electrochem. Soc.*

131, 11823 (1984).

<sup>9</sup>J. R. Dahn, M. A. Py, and R. R. Haering, *Can. J. Phys.* **60**, 307 (1982).

<sup>10</sup>W. R. McKinnon and J. R. Dahn, *Solid State Commun.* **52**, 245 (1984).

<sup>11</sup>R. Flukiger, R. Baillif, and J. Muller, *J. Less-Common Met.* **72**, 193 (1980); R. Schollhorn, M. Kumpers, A. Lerf, E. Umlauf, and W. Schmidt, *Mater. Res. Bull.* **14**, 1039 (1979); M. Tovar, L. E. DeLong, D. C. Johnston, and M. B. Maple, *Solid State Commun.* **30**, 551 (1979).

<sup>12</sup>W. R. McKinnon and J. R. Dahn, *Phys. Rev. B* **31**, 3084

(1985).

<sup>13</sup>C. Kittel and H. Kroemer, *Thermal Physics* (Freeman, San Francisco, 1980), 2nd ed.

<sup>14</sup>W. R. McKinnon, J. R. Dahn, and C. C. H. Jui, to be published.

<sup>15</sup>K. Yvon, in *Current Topics in Materials Science*, edited by E. Kaldis (North-Holland, Amsterdam, 1979), Vol. 3, p. 53.

<sup>16</sup>J. M. Tarascon, personal communication.

<sup>17</sup>R. B. Griffiths and J. C. Wheeler, *Phys. Rev. A* **2**, 1047 (1970).